P 453

Ytterbium-Doped Silica Fiber Lasers: Versatile Sources for the 1–1.2 μm Region

H. M. Pask, Robert J. Carman, David C. Hanna, Anne C. Tropper,
Colin J. Mackechnie, Paul R. Barber, and Judith M. Dawes

Invited Paper

Abstract— Ytterbium-doped silica fibers exhibit very broad absorption and emission bands, from ~800 nm to ~1064 nm for absorption and ~970 nm to ~1200 nm for emission. The simplicity of the level structure provides freedom from unwanted processes such as excited state absorption, multiphonon nonradiative decay, and concentration quenching. These fiber lasers therefore offer a very efficient and convenient means of wavelength conversion from a wide variety of pump lasers, including AlGaAs and InGaAs diodes and Nd:YAG lasers. Efficient operation with narrow linewidth at any wavelength in the emission range can be conveniently achieved using fiber gratings. A wide range of application for these sources can be anticipated. In this paper, the capabilities of this versatile source are reviewed. Analytical procedures and numerical data are presented to enable design choices to be made for the wide range of operating conditions.

I. INTRODUCTION

AFTER the first report in 1962 of laser action in Yb^{3+}-doped silicate glass [1], Yb^{3+} has, until recently, attracted relatively little interest as a laser-active ion. It has been overshadowed by the Nd^{3+} ion with its important advantage of a four level transition, whereas Yb^{3+} has only three level and quasi-three level transitions. In fact, the most important role of the Yb^{3+} ion has so far been as a sensitizer ion, absorbing pump photons over a wide spectral range and then transferring the excitation to an acceptor ion, such as Er^{3+}, which then acts as the laser-active ion [2], [3].

More recently, interest has been shown in Yb^{3+} as a laser ion, in the form of Yb^{3+}-doped silica and fluoride fiber lasers [4]–[8], and Yb^{3+}-doped YAG [9], [10]. There are several reasons for this growth of interest. As shown in Fig. 1(a), the Yb^{3+} energy level structure is a simple one, consisting of two manifolds; the ground manifold $^2F_{7/2}$ (with four Stark levels labeled (a)–(d) in the figure) and a well-separated excited manifold $^2F_{5/2}$ (with three Stark levels labeled (e)–(g) in the figure), ~10 000 cm^{-1} above the ground level. Thus there is no excited state absorption at either pump or laser wavelengths. The large energy gap between $^2F_{5/2}$ and $^2F_{7/2}$ precludes

nonradiative decay via multiphonon emission from $^2F_{5/2}$, even in a host of high phonon energy such as silica, and also precludes concentration quenching. These features contribute to the high efficiency of operation that can be achieved in Yb^{3+} lasers, as does the closeness of the pump and laser wavelengths. In fact, this energy defect, which leads to heating of the host, is a factor of ~3 smaller for Yb:YAG compared to Nd:YAG (pumped at 800 nm and lasing at 1064 nm). This reduced thermal burden is a motivating interest for Yb:YAG. Finally, the Yb^{3+} spectrum is rather broad both in absorption and emission, and particularly so in a germanosilicate host, as shown in Fig. 1(b). The broad absorption spectrum allows a wide choice of pump wavelengths. In the form of a fiber, which allows even very weak absorption to be exploited, pumping can extend from 800 nm out to 1064 nm. Similarly, for a fiber, laser operation can be made to extend well into the weak wings of the emission, provided sufficient frequency discrimination can be introduced to suppress lasing at the peaks of the emission profile. The impressive progress in development of fiber gratings [11] has made this matter of frequency discrimination very straightforward and practical, so one can now contemplate the prospect of narrow linewidth operation at any discrete wavelength between ~975 and ~1200 nm, with some degree of tunability (~1)% available by stretching or temperature tuning the grating. This range covers a number of wavelengths needed for specific applications, and these can now be generated very conveniently from an Yb^{3+}-doped silica fiber equipped with appropriate gratings. Examples include 1020 nm for pumping 1300-nm fiber amplifiers [12] and upconversion lasers based on Pr^{3+}-doped ZBLAN [13]–[15], 1140 nm for pumping Tm^{3+}-doped ZBLAN upconversion lasers [16], [17], and 1083 nm for optical pumping of He [18].

Given the wide range of different operating characteristics that might be required for various applications, and the variety of ways (e.g., different pump wavelengths) that could be used to achieve these characteristics, there is a need for a comprehensive discussion of the capabilities of Yb^{3+} fiber lasers, giving quantitative design procedures. Such has been the aim of this paper. A general discussion of Yb laser characteristics is presented in Section II. In Section III, analytical procedures and numerical data are presented to enable design choices to be made. Such calculations depend heavily on the availability of accurate absorption and emission cross section data, and the relevant spectroscopy is described in Section IV.
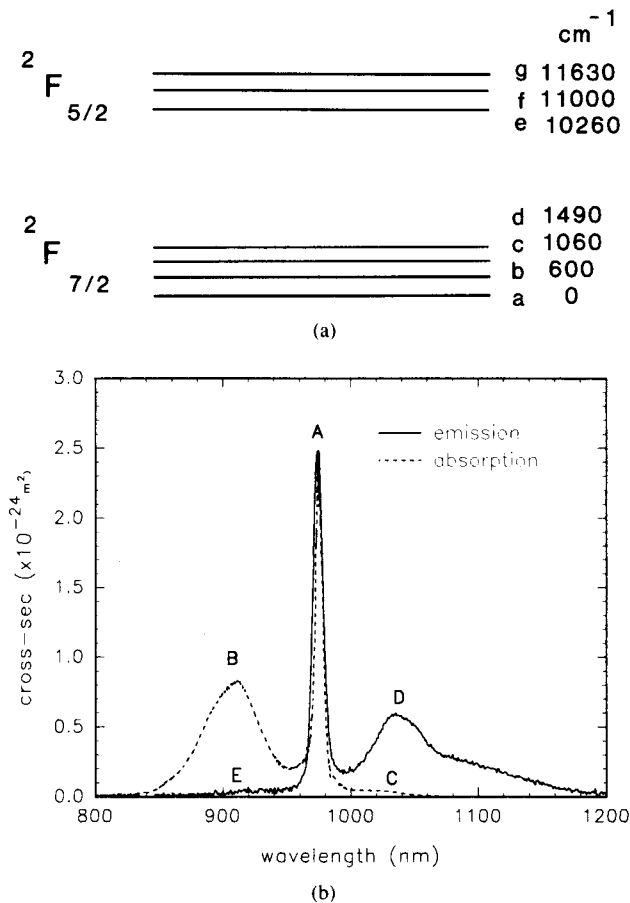
Fig. 1. (a) The Yb^{3+} energy level structure, consisting of two manifolds, the ground manifold $^2F_{7/2}$ (with four Stark levels, labeled (a)–(d)), and a well separated excited manifold $^2F_{5/2}$ (with three Stark levels labeled (e)–(g)). Approximate energies in wavenumbers above ground energy are indicated. (b) Absorption and emission cross sections for a germanosilicate host. The principal features of the spectra have been labeled A–E, and are discussed in the text.

In Sections V–VIII, some specific examples are drawn from both experimental and modeling studies of Yb^{3+}-doped silica laser action both to illustrate the agreement between modeling and experiment, and to illustrate the versatility and potential of this laser system.

II. GENERAL DISCUSSION

The most obvious features of the absorption and emission spectra in Fig. 1(b) have been labeled (A)–(E). The narrow line at 975 nm (A) in both absorption and emission, corresponds to transitions between the lowest Stark levels in each manifold. The absorption peak at shorter wavelengths (B) corresponds to transitions from level a to f and g, while the long wavelength shoulder in the absorption spectrum (C) corresponds to transitions from level b. The weakness of this shoulder is a consequence of the much smaller population of this level (~6% of level a at room temperature, as calculated from the Boltzmann factor). Despite the weakness of this shoulder, it plays a significant role. First, it provides the means for pumping using a Nd:YAG or Nd:YLF laser (at 1064 or 1047 nm respectively) [7]. Second, it is a cause of reabsorption

loss, having a significant effect on threshold for lasing at wavelengths within the dip in the emission spectrum.

Laser action on the narrow peak at 975 nm (A), where emission is into the lowest Stark level, is truly three-level in character. The second peak in the emission spectrum (D), with its tail extending out to 1200 nm, corresponds to transitions from level e to b, c, and d. Laser action on these transitions becomes nearly four level in character at longer wavelengths, as the emission is into essentially empty levels c and d. Transitions from level f are also evident (E), although very weak due to the small thermal population of the level, and laser action has not been observed on transitions from that level.

In general, when generation of a particular laser emission wavelength is required, there is a wide choice of possible pump wavelengths ranging from ~800 to ~1064 nm, and therefore, a choice of pump laser sources including AlGaAs and InGaAs diodes, Titanium sapphire lasers, Nd:YLF lasers and Nd:YAG lasers. As will be demonstrated in subsequent sections, extremely efficient laser action can be achieved using any of these sources. There are, however, several considerations other than the availability of sources that can go into the choice. First, one can only generate gain and hence lasing at longer wavelengths than the pump, so for example, 1020-nm operation cannot be achieved with a 1064-nm pump, but can with 975 nm pumping into the sharp absorption line. Second, pumping at 975-nm accesses the largest absorption cross section, so this is particularly appropriate where the shortest fiber length is required as for example in a single frequency laser. It is also appropriate for cladding-pumping, enabling the fiber length to be kept down to reasonable values, since the cladding-pumping geometry involves a scaling up of the absorption length, as described in Section VII. When pumping at 975 nm, it may be important to consider the effects of amplified spontaneous emission (ASE), as discussed below. Third, the slope efficiency with respect to absorbed pump power of Yb^{3+} lasers is usually dominated by the ratio of laser to pump photon energies. It is therefore possible to significantly enhance the conversion efficiency (e.g., by up to ~20% for laser action at 1140nm) by pumping close to the laser wavelength (e.g., with a Nd:YLF or Nd:YAG laser). Fourth, the pump power requirements are a function of the absorption and emission cross sections at the pump wavelength.

The critical pump power P_{cr} required to achieve a gain coefficient of zero at a particular point in the fiber (i.e., to reach transparency for the signal/laser wavelength), is given by

$$P_{cr} = \frac{Ah\nu_p}{\tau} \frac{1}{\left(\frac{\sigma_{el}\sigma_{ap}}{\sigma_{al}} - \sigma_{cp}\right)}.$$

Here we have assumed no background loss in the fiber. This expression can be readily derived from (2)–(5) in the next section, when the gain coefficient, $g(z)$, is set equal to zero and the pump quantum efficiency is assumed to equal unity. A, h, ν_p, and τ denote the core area, Planck's constant, pump laser frequency, and upper level lifetime respectively, σ_{el} and
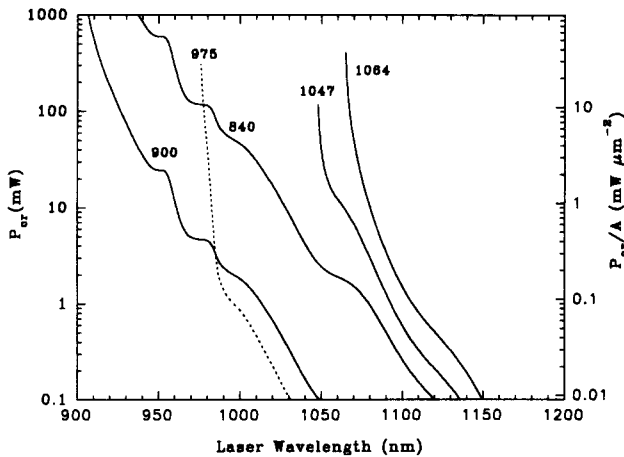
Fig. 2.   Calculated values of the critical pump powers (for a 3.75μm diameter fiber) and intensities required to produce net gain (i.e., to reach transparency for the signal wavelength) in Yb^{3+}-doped silica fiber, plotted as a function of signal (lasing) wavelength and for various pump wavelengths.

σ_{al}, the emission and absorption cross sections at the laser wavelength, and σ_{ep} and σ_{ap}, the emission and absorption cross sections at the pump wavelength, respectively. The critical power is independent of Yb^{3+} concentration, and whatever the fiber length or dopant concentration, for most efficient use of pump power, either at or above threshold, the power emerging from the fiber end (neglecting the Fresnel reflection) would, in fact, be equal to this critical power. Fig. 2 shows the critical power and also the corresponding intensities (for a typical fiber with diameter 3.75-μm) plotted as a function of lasing wavelength for various pump wavelengths of interest. This figure is useful in making design choices, as it can be seen that the critical powers are quite high for some combinations of pump and laser wavelengths. For example, to achieve lasing at 975 nm, it would be preferable to use a 900-nm pump source rather than an 840-nm pump source.

To further illustrate the dependence of lasing wavelength on pump conditions, we show the calculated gain spectrum for the specific case of pumping at 840 nm in Fig. 3(a). For low pump powers (5 mW) in the illustrated example, net gain first appears at long wavelengths $\sim$1100 nm for which there is negligible reabsorption from population in the lower level. Then, as pump power increases, the gain maximum moves progressively to shorter wavelengths, with the pure three level transition eventually having the dominant gain. The oscillation wavelengths under free-running conditions, i.e., without any wavelength selection applied, will correspond to the wavelength which has peak gain at the threshold for oscillation. With progressively harder pumping above threshold, assuming pure homogeneous broadening, the emission wavelength should remain clamped at its threshold value.

Some degree of control over the free-running wavelength can be achieved by changing the Q of the resonator, or by changing the fiber length. Changing the Q of the resonator changes the required gain for threshold, and therefore, the wavelength of peak gain, as can be seen in Fig. 3(a). Fig. 3(b) shows the gain under the same conditions as in Fig. 3(a), but with a fiber which is 20 times longer. The gain maxima are
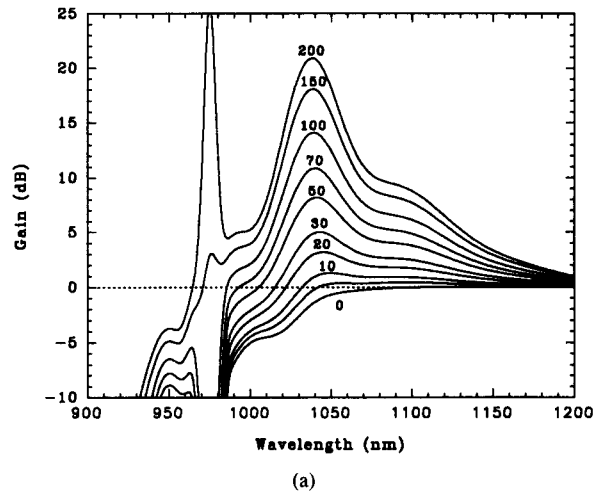
(a)
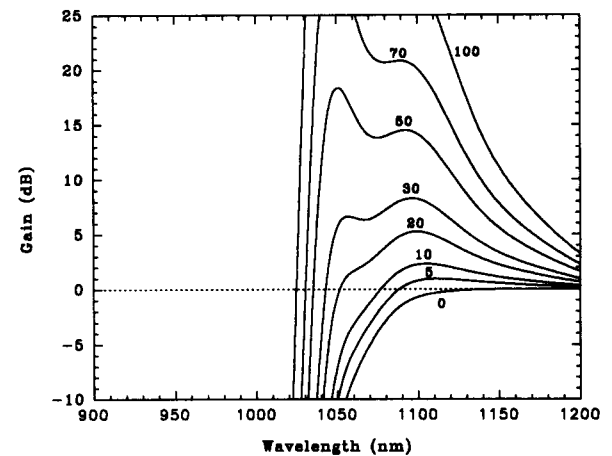
(b)

Fig. 3.   Calculated gain spectrum for the specific case of pumping at 840 nm for two fiber lengths (a) 1 m, (b) 20 m. (fiber diameter 3.75 μm, NA$\sim$0.17, [Yb^{3+}]$\sim$550 ppm). Curves are labeled with the launched pump power in milliwatts.

moved to longer wavelengths as a result of reabsorption in the extra length of fiber (e.g., compare the 30 mW curves in both figures). Thus oscillation at shorter wavelengths, e.g., at the 975 nm or 1040 nm gain peaks, can be suppressed by using a longer fiber to introduce reabsorption at these wavelengths. Alternatively one can use a longer pump wavelength (e.g., 1064 nm) than 975 nm or 1040 nm, thus ensuring no gain at these emission peaks. In this case a longer fiber is also needed, not to suppress the gain at 975 nm, but to ensure adequate absorption of the pump. While these two approaches both lead to the suppression of 975-nm gain, there is a difference which could become important under some circumstances. This is where short wavelength pumping is used and a very high gain at 975 nm is established at the input end of the fiber, although with net gain at 975 nm over the entire fiber length being suppressed by reabsorption further down the fiber. Under appropriate conditions strong ASE at 975 nm or even at $\sim$1040 nm could occur, and while the ASE travelling down the fiber would be reabsorbed and simply lead to a redistribution of the gain, the ASE that escapes from the input end would result in a loss of pumping efficiency and hence higher thresholds.

Data such as those presented in Fig. 3 are also useful in indicating the degree of frequency discrimination needed to enforce oscillation at wavelengths away from the free-running wavelength. Thus, from the data in Fig. 3(a) it is seen that to achieve oscillation at 1020 nm for a threshold pump power of 50 mW it is necessary to introduce $\sim$5 dB of discrimination against 1040 nm to suppress its oscillation. Under higher gain conditions, i.e., for higher pump powers, the degree of frequency discrimination required can be seen to increase. As a general point, it should be noted that if the peak gain becomes high enough to allow strong ASE ($\sim$30-40 dB single-pass gain), then frequency discrimination via end reflectors, however great, will become ineffective. It is therefore clear that when oscillation in the low gain region of the emission spectrum is required (at long wavelengths or in the dip between the emission peaks) it is necessary to use a resonator having low loss at the desired oscillation wavelength. Fiber gratings are particularly well-suited to this need as they can provide both a high frequency discrimination and a very high reflectivity and, when written directly into the doped fiber, introduce negligible insertion loss. For example, with appropriate gratings we have achieved oscillation out to 1180 nm, and with further optimization and reduction of losses this could, in principle, be extended somewhat further.

This preceding discussion has indicated some of the main features that need to be considered when designing an Yb fiber laser to operate under specific conditions, particularly with regard to pump and operating wavelengths. It is seen that it is important to make appropriate choices of fiber length and concentration, resonator Q, and the degree of frequency discrimination. The next section provides an analytical treatment of Yb^{3+} fiber lasers, from which calculated data, such as in Fig. 3, are generated.

III. CALCULATION OF GAIN

For simplicity, we assume pump and laser intensity profiles to be uniform over the area A of the core and also assume a uniform dopant distribution within the core. Steady-state conditions are also assumed. The total populations of the $^2F_{7/2}$ and $^2F_{5/2}$ manifolds are designated N_1 and N_2, respectively. The total population N is then

$$N = N_1 + N_2. \qquad (1)$$

Absorption $\sigma_a(\lambda)$ and emission $\sigma_e(\lambda)$ cross sections are defined such that the absorption coefficient at wavelength λ is $N_1\sigma_a(\lambda) - N_2\sigma_e(\lambda)$. For brevity we write $\sigma_a(\lambda_p)$ and $\sigma_e(\lambda_p)$ as σ_{ap} and σ_{ep} respectively, and $\sigma_a(\lambda_l)$ and $\sigma_e(\lambda_l)$ as σ_{al} and σ_{el}, respectively, where λ_p and λ_l are the pump and laser wavelengths, respectively.

The gain achieved in a length L is given by

$$\exp\left(\int_0^L g(z)\,dz\right) \qquad (2)$$

where $g(z) = N_2(z)\sigma_{el} - N_1(z)\sigma_{al}$. The value of $N_2(z)$ and hence $N_1(z) = N - N_2(z)$, is determined from the pump power $P_p(z)$ at that location. $P_p(z)$ obeys the equation

$$\frac{dP_p(z)}{dz} = -N_1\,\sigma_{ap}\,P_p(z) + N_2\,\sigma_{ep}P_p(z). \qquad (3)$$

Here we have assumed that background loss can be ignored. Our experimental results confirm that for fiber lengths up to $\sim$100 m the background loss (estimated at < 10 dB/km) played a negligible role.

To solve for $P_p(z)$ we make use of (1) and of the relation

$$\frac{dP_p(z)}{dz} = -\frac{A\,h\,\nu_p}{\phi_p\,\tau}\,N_2(z) \qquad (4)$$

where τ is the lifetime of the upper level and ϕ_p is the pumping quantum efficiency (in this case, for Yb^{3+}, $\phi_p \sim 1$).

From (1), (3), and (4) we obtain the result

$$\ln\left(\frac{P_p(z)}{P_p(0)}\right) + \frac{P_p(z) - P_p(0)}{P_s} = -N\sigma_{ap}z \qquad (5)$$

where $P_p(0)$ is the input pump power and P_s is the pump saturation power (i.e., the power that reduces the absorption coefficient by a factor of 2).

P_s is given by

$$P_s = \frac{h\nu_p\,A}{(\sigma_{ep} + \sigma_{ap})\,\tau\,\phi_p}. \qquad (6)$$

Thus, $P_p(z)$ can be calculated from (5).

The single-pass gain exponent (2) for a length l of fiber is then given by

$$(\sigma_{el} + \sigma_{al})\int_0^l N_2(z)dz - N\sigma_{al}l$$

which can be reexpressed with the help of (4) as

$$\frac{\phi_p(\sigma_{el} + \sigma_{al})\tau P_a}{Ah\nu_p} - N\sigma_{al}l \qquad (7)$$

where P_a is the absorbed power

$$P_a = P_p(0) - P_p(l). \qquad (8)$$

Thus, the procedure for calculation of gain reduces to calculating $P_p(l)$ from (5), hence, P_a (via (8)), and then the gain exponent from (7), or expressed in dB

$$\text{gain} = 4.34\left[\frac{\phi_p(\sigma_{el} + \sigma_{al})\tau P_a}{Ah\nu_p} - N\sigma_{al}l\right]\text{dB}. \qquad (9)$$

This expression simplifies if σ_{al} can be neglected, for example, for long wavelength operation, such as 1140 nm. Similarly, the expression for P_s is simplified when σ_{ep} is zero, as in the case where pumping is at short wavelengths, say less than 940 nm.

A generalization of the equations to deal with cladding-pumping is straightforward. If the area of the inner cladding into which the pump is launched is x times the area of the core, then the pump cross sections should be replaced throughout by σ_{ap}/x and σ_{ep}/x. Thus, the effective saturation intensity

becomes x times greater (6) and the right-hand side of (5) becomes $-N\sigma_{ap}z/x$.

The above analysis assumes that all the ions in the fiber are characterized by identical absorption and emission cross sections, i.e., that spectral broadening is homogeneous. The amorphous nature of a glass, however, leads to site-to-site variations of the local electric field, producing a degree of inhomogeneous broadening in the system. There is insufficient information available to accurately model the effect of any inhomogeneity. Spectral inhomogeneity could manifest itself in the form of spectral hole burning, either in pump absorption or laser emission. Since our analysis above is a small-signal analysis of the laser gain, however, the effects of spectral hole burning due to lasing can be neglected. They may, however, need to be considered for operation above threshold.

IV. SPECTROSCOPY

Successful modeling of the Yb^{3+} laser performance requires an accurate knowledge of the absorption and emission cross sections. The cross sections shown in Fig. 1(b) were determined experimentally, as described in this section.

The sidelight fluorescence spectrum was obtained, using an integrating sphere, from a length of fiber stripped of its protective jacket and pumped at 840 nm. The form of the emission cross section was determined by scaling the measured fluorescence spectrum by λ^5, and the absolute value of the emission cross section was then obtained by relating the integrated cross section to the measured upper level lifetime, using the relationship

$$W_{rad} = \frac{1}{\tau} = \frac{8\pi n^2}{c^2} \int \nu^2 \sigma_{em}(\nu) \, d\nu. \tag{10}$$

The decay of sidelight fluorescence from $^2F_{5/2}$ was measured by chopping the pump acoustooptically at ~ 60Hz. The fluorescence was collected by a bundle of fibers and imaged onto a silicon photodiode. The fluorescence decayed exponentially over the first three e-folds, with a decay time of ~ 840 μ's. The energy spacing between the two manifolds ($>10\,000$ cm^{-1}) greatly exceeds the maximum phonon energy in silica (~ 1100 cm^{-1}), and the observed fluorescence lifetime is taken to be the radiative lifetime.

The form of the absorption cross section was measured from the transmission of a white light source using a cut back technique. The well resolved peak at 975 nm that appears both in emission and absorption corresponds to transitions between the lowest energy Kramers doublets in the ground and excited manifolds. The absorption spectrum was scaled to give equal absorption and emission cross sections at the peak wavelength. This is an approximation, because the crystal field splitting is larger in the excited manifold than in the ground manifold and the degeneracy is lower; a McCumber analysis suggests that at room temperature the absorption cross section may be 5–10% larger than the emission cross section. This discrepancy is comparable with other experimental uncertainties. The profiles of the room temperature absorption and emission cross section spectra shown in Fig. 1(b) agree well with the McCumber relationship $\sigma_a = \sigma_e \exp(\epsilon - h\nu)$, where the free-energy

parameter ϵ was taken to be the energy difference corresponding to the sharp peaks (at 975 nm) in the absorption and emission spectra. An independent confirmation of this scaling was obtained from a measurement of fluorescence sidelight as a function of pump power. The pump power (at 1017 nm) required to reach half the maximum fluorescence intensity (pump saturation power) is given by (6). This measurement gave a value for $(\sigma_a + \sigma_e)$ of 0.43 ± 0.1 pm^2, in fair agreement with the value obtained from the absorption and emission cross sections (0.39 pm^2). This result justifies the assumption that the $^2F_{5/2}$ lifetime is predominantly radiative.

To determine the concentration of Yb^{3+} in the fibers used, cutback measurements were performed using low incident powers. Assuming a Beer's law distribution of pump power along the fiber, the small-signal absorption coefficient was deduced which is the product of the dopant concentration, cross section, and overlap integral of the pump with the dopant. The overlap integral is not easily calculated; the distribution of the dopant across the fiber core tends to follow the germania distribution and varies with fiber drawing conditions. Therefore, we have chosen to work with an effective concentration, i.e., the product of the concentration and overlap integral. The effective concentration estimated in this way is 550 ± 100 ppm.

V. OPERATION AS A FREE-RUNNING LASER

In this section, the operating characteristics of single-spatial-mode, free-running Yb^{3+} lasers are presented. The results have been chosen to illustrate the versatility and general principles of laser action in Yb^{3+}-doped silica fibers and to show the agreement between theory and experiment. The Yb^{3+}-doped germanosilicate fibers used for these experiments had numerical aperture ~ 0.17, and dopant concentration ~ 550 ppm, and diameters of either 3 μm or 3.75 μm. The background loss was found to be < 10 dB/km. Pump light, from either a Ti-sapphire laser, Nd:YLF or Nd:YAG laser was launched into the fiber using a x10 or x16 microscope objective, and laser action was investigated for resonators with feedback provided by two bare, cleaved fiber ends, or one cleaved end and a butted dielectric-coated mirror at the other end. Typical launch efficiencies varied from ~ 50% for the Ti-sapphire laser to ~ 70% for the Nd:YLF laser.

Laser action has been investigated for pumping at wavelengths from 840–1064 nm. In all cases, very efficient laser operation can be achieved, with slope efficiencies of up to 90% with respect to absorbed power. Depending on the fiber length and optical feedback, laser operation has been demonstrated from 1035–1115 nm.

In Fig. 4, the results of modeling calculations (line) are compared with measurements (symbols) of threshold powers and lasing wavelength as a function of fiber length. Threshold powers (Fig. 4(a)) are in terms of launched pump power, and the calculated thresholds are seen to be within 30% of the measured thresholds. The trends predicted by the modeling are confirmed by the experimental measurements.

There is clearly an optimum length for reaching threshold for laser action at low values of launched pump powers, and this represents a compromise between maximizing pump absorption and minimizing the reabsorption losses at the laser
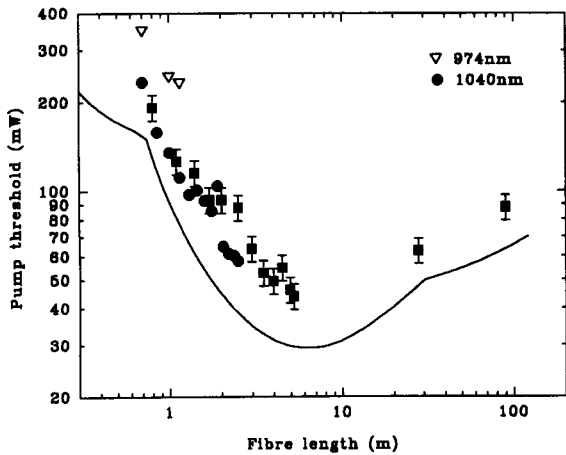
(a)
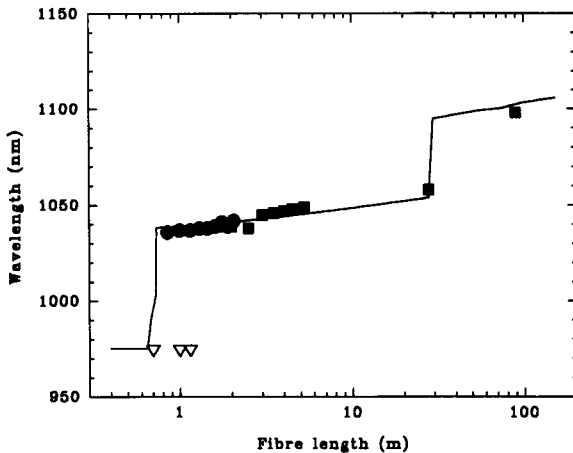
(b)

Fig. 4. Some results of modeling calculations (lines) are compared with measurements (symbols) of (a) threshold powers and (b) laser wavelength as a function of fiber length. Threshold powers are in terms of launched pump power (fiber diameter 3.75 μm, NA$\sim$0.17, [Yb^{3+}]$\sim$550 ppm, pump wavelength 840 nm)

wavelength. The laser wavelength shifts to longer values as the fiber length is increased, as a consequence of the tail in the absorption spectrum which extends toward 1100 nm. This was discussed in Section II.

Despite the increased threshold for the longer fiber lengths, it is possible to obtain very efficient laser action in lengths up to 90 m. This is illustrated in Fig. 5, where laser performance is shown for fiber lengths of 8, 28, and 90 m, pumped at 850 nm with feedback provided by Fresnel reflections from the cleaved fiber ends. For these lengths the slope efficiencies were 70–80% with respect to launched pump power. For fiber lengths over 90 m the laser wavelength remains at 1090 nm. The laser wavelength can be changed by varying the amount of optical feedback, as discussed in Section II. For the three fiber lengths shown in Fig. 5, a highly-reflecting mirror was butted to the output end of the fiber, and this was found to shift the laser wavelength from 1038 to 1050 nm for the 8 m length, 1058 to 1060 nm for the 28 m length and 1090 to 1106 nm for the 90 m length. This behavior was also predicted by the modeling. Noticeable features of the laser characteristics in Fig. 5 are the soft thresholds, a characteristic of quasi-three level laser systems, discussed in detail by Fan and Byer [19].
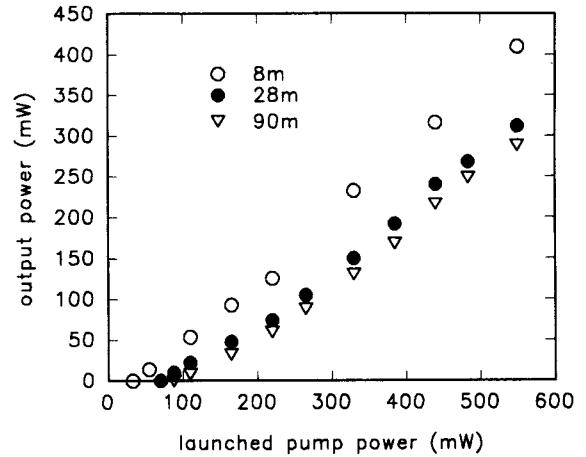

Fig. 5. Free-running laser performance for three fiber lengths: 8, 28 and 90 m, pumped at 850 nm. Feedback is provided by Fresnel reflections from the cleaved fiber ends (fiber diameter 3.75 μm, NA$\sim$0.17, [Yb^{3+}]$\sim$550 ppm).

In all of the examples we cite in this paper, laser performance has been investigated for pump powers up to many times above threshold, in which case, to extract maximum power it is more important to maximize the slope efficiency than to minimize threshold. Consequently, the fiber lengths used experimentally tend to exceed the optimum lengths for minimizing threshold, as determined from the modeling, so as to ensure that virtually all of the launched pump power is absorbed.

Very efficient laser performance has been demonstrated when pumping at 1064 and 1047 nm [7]. Due to the very weak absorption of the pump at these wavelengths (only $\sim$0.1 dB/m at 1064 nm for our 550 ppm doping level), it is necessary to use long fiber lengths, typically $\sim$100 m, to obtain efficient pump absorption. Because of the closeness of pump and lasing wavelengths, however, extremely high slope efficiencies (>90)% can be achieved. For example Fig. 6 shows the performance at 1102 nm demonstrated using a 90 m length of fiber, with one end cleaved and a mirror at the launch end which transmitted at 1047 nm and was highly-reflecting at 1102 nm. The threshold for laser action occurred for 30 mW launched pump power, and the slope efficiency was over 90% with respect to launched pump power. It is interesting to note that the laser wavelength, when such long fiber lengths are used, is essentially independent of pump wavelengths from 840 nm to 1064 nm. The scaling of Yb^{3+} lasers to higher powers has also been addressed, and output powers as high as 2W at 1090 nm have been demonstrated by using a CW lamp-pumped laser at 1064 nm to pump a 90 m length of fiber with two bare ends. No sign of rollover in the laser performance and no damage to the fiber were observed at these power levels. These results illustrate that Yb^{3+} lasers offer an extremely efficient way of converting high power Nd:YAG or ND:YLF lasers to longer wavelengths, particularly when using fiber gratings to select particular lasing wavelengths, as described in the next section.

VI. OPERATION AT SPECIFIC WAVELENGTHS USING FIBER GRATINGS

To achieve oscillation outside the band of wavelengths accessible by free-running cavity configurations, and also to
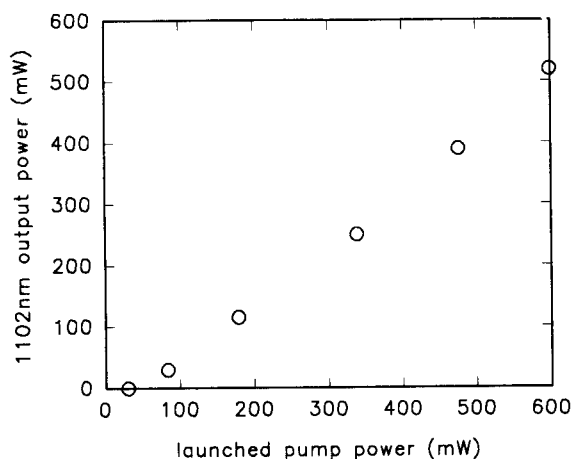
Fig. 6. Free-running laser performance obtained using a 90 m length of fiber. Feedback provided by a mirror at the launch end (R>98% at 1100 nm) and a cleaved fiber end (fiber diameter 3.75 μm, NA$\sim$0.17, [Yb^{3+}]$\sim$550 ppm, pump wavelength 840 nm).
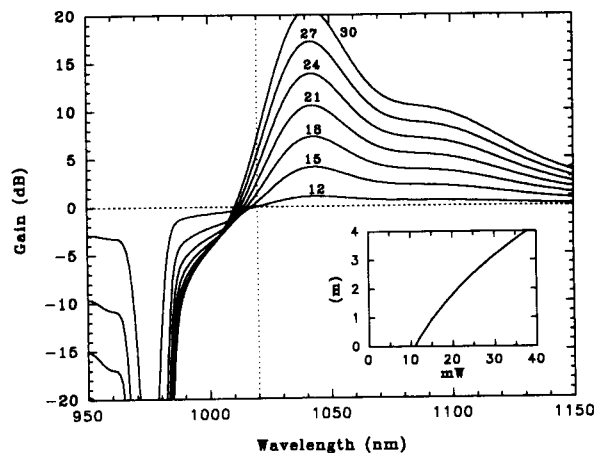

Fig. 7. Results of computer modeling, showing gain spectra for various values of launched pump powers, with the fiber length chosen to maximize available gain at 1020 nm. Optimum fiber length as a function of pump power is shown in the inset (fiber diameter 3.0 μm, NA$\sim$0.17, [Yb^{3+}]$\sim$550 ppm, pump wavelength 840 nm).

maintain maximum flexibility in choice of pump wavelengths and cavity length, it is often desirable to introduce some form of wavelength discrimination into the cavity. The use of bulk elements such as prisms and gratings together with the necessary intracavity lenses introduce losses which cause significant decreases in laser efficiency. A much more attractive approach to achieve efficient laser operation at any wavelength within the emission band is to incorporate fiber gratings [20] into the laser cavity [8]. The recent availability of photorefractive fiber gratings has been a major element in expanding the potential of Yb^{3+}-doped fiber devices. Laser action has been investigated at several wavelengths across the emission spectrum, and in this section we present the performance characteristics of Yb^{3+}-doped silica lasers operating at 1020 nm and at around 1140 nm, together with modeling results. The modeling is particularly useful in predicting the amount of selectivity required to suppress oscillation at free-running wavelengths.

For our experiments, gratings having reflectivities up to 99% at any wavelength across the Yb emission spectrum have been fabricated in undoped photosensitive silica fiber using a line-narrowed KrF excimer laser. The gratings are written into the core of the fiber by UV illumination with two interfering beams through the cladding of the fiber [11], [20]. These gratings are then fusion-spliced to the Yb-doped silica fiber. More recently, gratings fabricated directly in the Yb^{3+}-doped fiber itself have been used.

A. Laser Action at 1020 nm

A practical source is required at 1020 nm for pumping 1300 nm Pr^{3+}-doped fluoride fiber amplifiers, and also for pumping Pr^{3+}-doped ZBLAN upconversion lasers. In Yb^{3+}-doped silica, however, larger gains are always available at longer wavelengths. This is illustrated in Fig. 7 by the results of computer modeling, which show gain spectra for various launched pump powers, with the fiber length optimized to give the maximum available gain at 1020 nm. By comparing the gains at the wavelength of interest, and at the wavelength of

peak gain, the amount of discrimination required to suppress the free-running wavelength can be deduced.

Laser action at 1020 nm has been demonstrated experimentally using fiber gratings to provide the necessary discrimination against the free-running wavelength (1050 nm). A 10 m length of 3.0 μm diameter fiber was pumped by the 840nm output from a Ti-sapphire laser. Gratings having reflectivities of $\sim$95% and $\sim$30% at 1020 nm were spliced to the input and output ends of the Yb^{3+}-doped fiber respectively. The round-trip output coupling loss is therefore 5.4 dB, i.e., equivalent to 2.7 dB single-pass loss. Each splice was measured to have a single-pass loss of 5% (0.22 dB), and therefore the single-pass gain required to reach threshold for lasing is $\sim$3.1 dB. For threshold to be reached at the free-running wavelength (with feedback from cleaved fiber ends) a single-pass gain of $\sim$15 dB is required, and the grating resonator used therefore provides $\sim$12 dB of discrimination. In practice it was found that angle-polishing of the fiber input end and the use of a Faraday isolator between the fiber laser and Ti-sapphire lasers helped to suppress the free-running wavelength. In general, the suppression of feedback at the wavelength of peak gain is an important precaution for achieving reliable operation at other wavelengths for which a large discrimination is needed.

Laser performance at 1020 nm is shown in Fig. 8. The threshold for laser action occurred for 55 mW of launched pump power, and for 510 mW of launched pump power, the output from the fiber consisted of 240 mW at 1020 nm, and 30 mW of unabsorbed pump light. The slope efficiency of this laser is $\sim$60% with respect to absorbed power. The splice losses account for the difference between measured slope efficiency and the ratio of laser to pump photon energies (82)%. This performance could be improved by fabricating the gratings directly into doped fiber, thereby eliminating the splice losses.

Laser output at 1020 nm has been used to pump a Pr-doped ZBLAN upconversion fiber laser. The excitation scheme requires two pump wavelengths at around 840 nm and 1020 nm, and a convenient dual wavelength source for this application
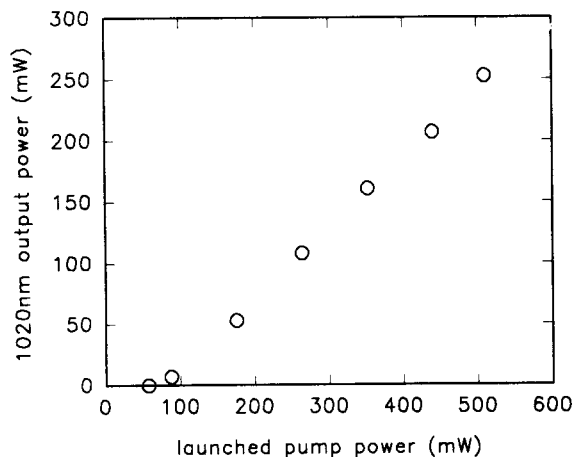
Fig. 8. Laser performance at 1020 nm achieved using fiber gratings. Feedback provided by gratings with reflectivities of ~95% and ~30% at 1020 nm spliced to the input and output ends of the Yb^{3+}-doped fiber respectively (fiber length 10m, diameter 3.0 μm, NA~0.17, [Yb^{3+}]~550 ppm, pump wavelength 840 nm).

has been developed using a 5 m length of 3.0-μm diameter fiber, which was chosen to give equal amounts of unabsorbed pump (840 nm) and laser output (1020 nm). This output was used to pump a Pr^{3+}-doped ZBLAN upconversion fiber laser from which, when provided with mirrors for blue, green, or red lasing, 6.5 mW at 491 nm, 18 mW at 520, and 55 mW at 635 nm were generated for a combined incident pump power of 380 mW at the two wavelengths [15].

B. Laser Action at 1140 nm

Another wavelength of particular interest is 1140 nm, required for pumping the efficient blue laser source based on upconversion in Tm^{3+}-doped fluoride fiber. Laser action at 1140 nm has therefore been investigated in Yb^{3+}-doped fiber using fiber gratings, and in this case using a diode-pumped Nd:YLF laser operating at 1047 nm as the pump source [17]. The computer-modeling in Fig. 9 shows gain spectra calculated for various launched pump powers. For each spectrum, the fiber length was optimized to maximize the gain at 1140 nm. As described in previous sections, the long fiber lengths (~100 m) required, are a consequence of the very weak absorption of the pump.

Laser action has been demonstrated at 1140 nm in a laser cavity consisting of a highly-reflecting dielectric-coated mirror butted to the input end of a 90 m length of 3.75-μm diameter doped fiber and a grating (~50% reflectivity at 1140 nm) written into a short length of the doped fiber and fusion spliced at the output end. The amount of discrimination provided against the free-running wavelength (1106 nm) was therefore ~4 dB per pass, and it was found that this was sufficient to constrain laser oscillation to 1140 nm. As shown in Fig. 10, the laser threshold was reached with only 6 mW of launched pump power, and 330 mW of output power was achieved for an launched pump power of 500 mW. The slope efficiency of the laser, with respect to launched pump power was ~66%; the difference between this and the limiting value of the ratio of laser to pump photon energies (92)%, probably
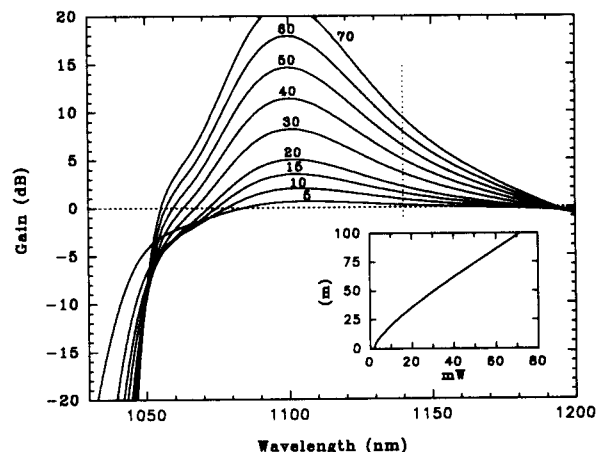

Fig. 9. Gain spectra calculated for various launched pump powers, with the fiber length chosen to maximize gain at 1140 nm as shown in the inset (fiber diameter 3.75 μm, NA~0.17, [Yb^{3+}]~550 ppm, pump wavelength 1047 nm).
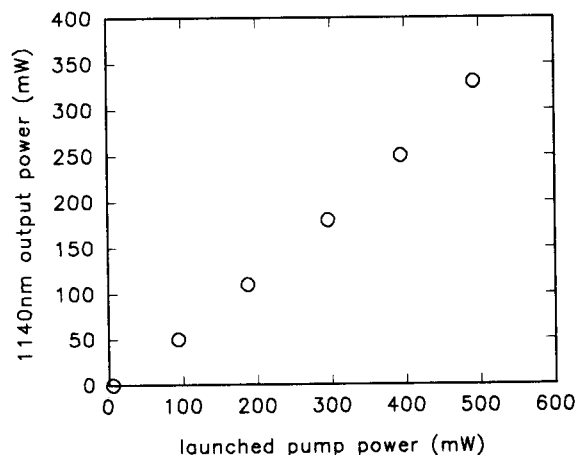

Fig. 10. Laser performance at 1140 nm achieved using a fiber grating. Feedback provided by a dielectric-coated mirror (99% reflectivity at 1100-1200 nm) and a grating (50% reflectivity at 1140 nm) written into the doped fiber at the output end (fiber length 100 m, diameter 3.75 μm, NA~0.17, [Yb^{3+}]~550 ppm, pump wavelength 1047 nm).

being due to the fiber background loss, mirror butt loss, and splice loss. This 1140 nm source has been used to pump a Tm^{3+}:ZBLAN upconversion laser, producing 30-mW output power at 480 nm [17].

VII. CLADDING-PUMPED OPERATION OF YB^{3+} LASERS

In previous sections we have presented results which illustrate that Yb^{3+}-doped fiber lasers are very efficient with respect to absorbed pump power. The overall conversion of incident pump light to laser output, however, is typically only ~40–60%, limited largely by the efficiency with which a near-diffraction-limited pump can be launched into single-mode fiber. In this section we consider the uses of cladding-pumping, which relaxes the requirements on pump beam quality and launch alignment, and which may find wider use, not just for Yb^{3+}-doped fibers, to get the highest launch efficiency for near-diffraction-limited pump sources. Another possible use for cladding-pumping would be to allow a much higher incident power than could be tolerated, for damage reasons,

with direct end-launching into the core. This is particularly relevant for pumping with Nd:YAG and Nd:YLF lasers for which very high power levels are available. With fiber grating reflectors in the core of such a fiber and a fiber taper at the output, such a laser could avoid the damage limitations imposed by dielectric mirrors or by the susceptibility of the fiber ends.

Cladding-pumping operates on the principle that the incident power is launched into and guided in the outer core (inner cladding). The dopant is confined within the inner core, and the absorption per unit length of pump light travelling in the outer core is therefore reduced by a factor approaching the ratio of the areas of the inner and outer cores. The reduced absorption per unit length, compared to direct core-pumping, is compensated for by using a combination of higher dopant concentration, longer fiber length, and a pump wavelength where there is strong pump absorption. The peak absorption in Yb^{3+}-doped silica occurs at 975 nm, and fortuitously, this is a wavelength at which a variety of InGaAs diodes are available. Cladding-pumping of Yb^{3+} fiber is therefore an attractive approach to achieving high output powers from compact, diode-pumpable devices.

In this section, we consider two applications of cladding-pumping which illustrate its uses and some of the considerations which are made in the design of cladding-pumped fiber lasers, and we show how the fiber design can be matched to the characteristics of the pump source. First, experimental results are presented which show that cladding-pumping with a near diffraction-limited pump source enables extremely high conversion efficiencies (80% with respect to available pump power) to be obtained. Second, modeling studies have been undertaken which suggest that cladding-pumping with broad-stripe diode arrays should also be feasible.

A. Cladding-Pumping with a Near Diffraction-Limited Pump Source

Semiconductor MOPA devices, now available (Spectra Diode Labs SDL-5762-A6) at ~975 nm with power levels ~1W and good beam quality ($M^2 < 2$) offer a very attractive source for pumping Yb^{3+}-doped fiber lasers. To get the best efficiency it is important to achieve a very high launch efficiency. As a means to this, we have investigated a cladding-pumped design, for which we recently reported [21] very efficient operation when pumped by a Ti-Sapphire laser. The fiber used in those experiments was designed with a relatively small diameter for the outer core (inner cladding), as appropriate for a near diffraction limited pump, intended to achieve a 90% launch efficiency for a MOPA pump. To simulate the expected performance under MOPA pumping, the pump light from the Ti- sapphire laser was launched using a relatively low power (× 5) microscope objective, producing a focal spot diameter ($1/e^2$ width), estimated to be ~12 μm, i.e., significantly larger than the inner core but fitting into the outer core. The fiber used was fabricated by the MCVD technique and germanosilicate cores were employed to give the refractive index profile which had an inner core diameter of 4.25 μm, an outer core (inner cladding) of 12.75 μm, an
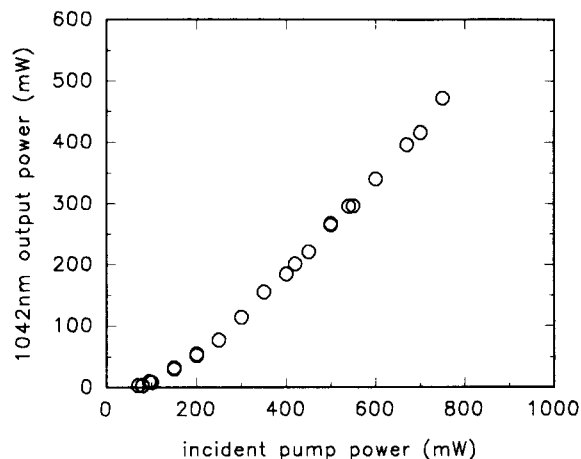
Fig. 11. Cladding-pumped laser performance at 1040 nm. Feedback provided by the cleaved fiber ends (fiber length 5 m, inner core diameter 4.25 μm, outer core (inner cladding) diameter 12.75 μm, NA (inner guide) ~.16, NA (outer guide) ~.15, [Yb^{3+}]~500 ppm.

NA for the inner guide of ~0.16 and an NA for the outer guide of ~0.15. Ytterbium was added to the inner core by solution-doping and the Yb^{3+} concentration is estimated to be ~500 ppm.

Laser performance at the free-running wavelength (1042 nm) is shown in Fig. 11. Optical feedback in this case was provided by the ~4% Fresnel reflections from the cleaved fiber ends. The fiber length was ~5 m, and only insignificant amounts of transmitted pump could be detected. Threshold for laser action was reached with 75 mW of pump power incident on the launch objective, and the slope efficiency was 80% with respect to incident power. This very high figure is the result of a very high launch efficiency, and is believed to be limited by the transmission of the launch objective (~95)%, the Fresnel reflection of the pump from the cleaved fiber end (~4)%, and the ratio of laser to pump photon energies (93.8)%. The launch efficiency of the pump was measured using a cut back technique to be ~90%. It was estimated, by launching into an un-doped single-mode fiber having a similar numerical aperture and core diameter to the inner guide, that less than 40% of the incident pump power was launched into the lowest order mode. The laser output was viewed with a beam profiler and its divergence measured, from which it was concluded that the fiber laser was operating on the lowest order mode for the structure.

It was demonstrated that photorefractive gratings could be written directly into the doped fiber core, as a result of the high GeO_2 content, enabling cladding-pumped operation at 1020 nm and 1140 nm to be achieved. For example, laser performance at 1020 nm was investigated in a 4 m length of fiber, into which fiber gratings having reflectivities of 62% and 37% at 1020 nm were written at the launch and output ends of the doped fiber respectively. Laser threshold was reached for 32 mW of incident pump power, and the slope efficiency for laser emission at the output end was measured to be ~42%, with respect to incident pump power. If, however, the laser emission from the launch end of the fiber is also considered, then the overall conversion efficiency is found to be ~70%.

The output beam, viewed with a beam profiler, was found to be confined to the lowest-order transverse mode.

Efforts aimed at optimization of the grating reflectivities, either in this fiber or in a more photosensitive fiber, are continuing with the expectation that laser efficiencies obtained using gratings will reach values close to that obtained in the free-running case. It is envisaged that this scheme could be applied to enable efficient conversion of 975 nm output from a semiconductor MOPA to any wavelength in the range 1000–1150 nm. It can also be used to lower the tolerances on pump beam quality and pump beam launch alignment. A higher Yb^{3+} concentration is also possible, and would be beneficial in reducing the fiber length required.

B. Cladding-Pumping with Diode Arrays

Cladding-pumping schemes have been successfully employed in the past to enable efficient pumping of single-mode cores with diode arrays [22]–[24]. As described in Section III, the equations used to calculate gain can readily be modified to predict cladding-pumped performance. The results of such calculations indicate that it should be feasible to demonstrate efficient operation by pumping with a diode array at 975 nm (e.g., Spectra Diode Labs model 6360).

The fiber design is influenced by three main considerations: 1) the need for a large NA for the outer guide to ensure efficient launching of the highly-divergent diode array output; 2) the need for a large inner core diameter to ensure a short absorption length (and hence reduced losses), while the NA for the inner core must be small enough to ensure single-mode operation of the fiber laser; 3) a high Yb^{3+} concentration, to also ensure a short fiber length. The fiber design is also, of course, constrained by what it is feasible to fabricate. The modeling calculation uses an Yb^{3+} concentration of ~1000 ppm although somewhat higher concentrations can be incorporated in practice. The calculation has been based on a particular fiber design, pumped at 975 nm, where the pump absorption is highest. There is, however, plenty of scope for variation of the fiber design and for choice of different pump wavelengths, for example, using the broad 920 nm absorption peak. If the numerical aperture of the inner cladding (outer core) is ~0.35 and its diameter is 120 μm, then it should be possible to couple at least 50% of the output from the diode array into the fiber. With a V value of 2.405 at 1.14 μm and NA of 0.13, the diameter of the inner core becomes 6.8 μm. These dimensions define the outer-inner core area ratio to be $x = 311$, a number which determines the minimum effective pump absorption length (i.e., the absorption length assuming efficient mixing of modes).

The results of a typical calculation are presented in Fig. 12. Each curve pertains to a different value of launched pump power. The pump power required to reach threshold at the wavelength of peak gain is predicted to be ~10 mW for a cavity where the losses are ~3 dB. On the grounds of previous work, the slope efficiency with respect to launched pump power is expected to exceed 70% provided the fiber is long enough to absorb all of the incident power, and the fiber losses do not exceed 10 dB/km. Assuming a launch efficiency of 50%, it should be possible to obtain ~350 mW at ~1100 nm
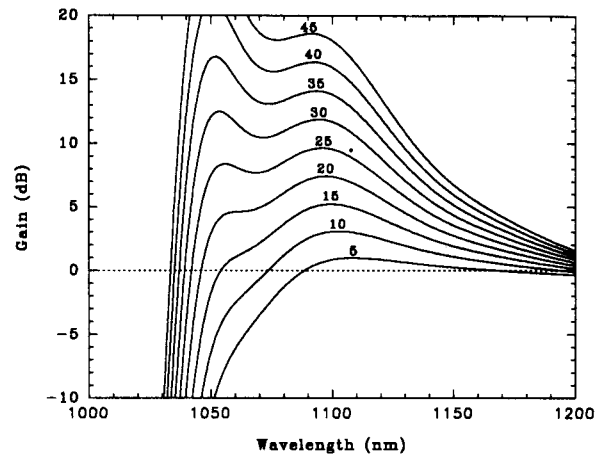

Fig. 12. Typical results of a cladding-pumping calculation, showing gain spectra for various launched pump powers (fiber length 15 m, inner diameter 6.8 μm, outer diameter 120 μm, $[Yb^{3+}]$~1000 ppm, pump wavelength 975 nm).

in a single transverse mode, by pumping with a 975-nm diode array.

The wavelength of greatest gain depends on the pump power and the fiber length, as discussed in previous sections. It is also predicted that efficient cladding-pumped operation should be possible at wavelengths where the gain is lower, using fiber gratings. As described in Section VI, the calculations indicate the amount of discrimination required to suppress the free-running wavelength; Fig. 12 suggests that the range 1050–1150 nm could be covered with ease. At the input end of the cladding-pumped fiber one could use a dielectric multilayer mirror. The required amount of discrimination could readily be achieved by using a fiber grating, which could be fabricated in a separate undoped photosensitive fiber which is mode-matched to the inner guide and fusion-spliced to the output end of the cladding-pumped fiber. It is highly desirable for the fiber to have low propagation losses at both pump and signal wavelengths. This not only achieves a low laser threshold, but equally importantly ensures a low laser gain, so that one fiber grating can readily achieve the necessary discrimination against lasing at the peak of the gain curve.

VIII. SINGLE-FREQUENCY LASER OPERATION

As described elsewhere [25], [26], efficient single-frequency operation can be achieved using simple, short, linear cavities incorporating fiber Bragg gratings to provide both cavity feedback and longitudinal mode discrimination. Such operation has been demonstrated at 1500 nm in Er [25] and Er/Yb [26] fibers. We have recently obtained [27] preliminary results which demonstrate that Yb^{3+}-doped fiber lasers are promising narrow linewidth sources for the 1000–1150-nm spectral region. The specific wavelength of operation, 1083 nm, was chosen on the basis of its usefulness for Helium pumping [18].

Relatively high dopant concentrations are required for efficient operation using short cavities. The fiber fabricated for this work had an Yb^{3+} concentration of ~2000 ppm, NA~0.28, and a cut off wavelength ~1000 nm. No evidence of concentration quenching was observed. The fiber was
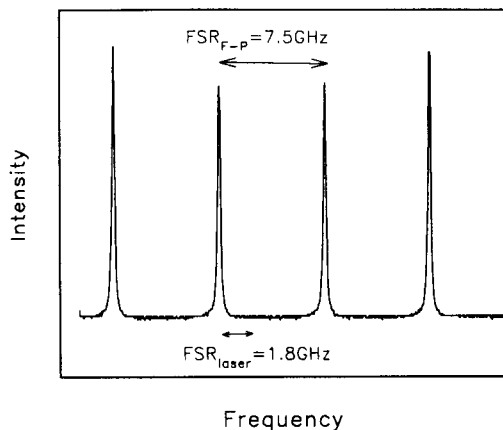
Fig. 13. Output from scanning confocal Fabry–Perot interferometer demonstrating single-longitudinal mode operation. Interferometer FSR~7.5 GHz, laser FSR~1.8 GHz, and instrument-limited bandwidth ~200 MHz.

designed to allow direct writing of high reflectivity, narrow-band gratings into the doped fiber core, thereby eliminating the need for intracavity splices. The fiber ends can either be cleaved or angle-polished, thereby permitting a number of coupled-cavity configurations to be designed [28]. The entire length of the laser cavity could be pumped uniformly, depending on the choice of pump wavelength.

Stable single-frequency operation at 1083 nm was obtained using a 5.6-cm long cavity formed by two gratings with reflectivities of 92% and 60%, respectively at the launch and output ends. The reflectivity bandwidth, at full width half maximum, was 0.25 nm for each grating. Pump light at 970 nm from a Ti-sapphire laser was launched into the cleaved end of the pigtail (~1 cm long) at the launch end, and laser action at 1083.0 nm on a single longitudinal mode occurred with a threshold of ~12-mW pump light incident on the launch objective. Single-frequency operation was verified using a scanning confocal Fabry–Perot interferometer with 7.5-GHz free spectral range (FSR) and instrument-limited bandwidth of ~200 MHz. The output from the interferometer is shown in Fig. 13. The FSR of the laser was ~1.8 GHz. The slope efficiency for these initial measurements was ~6% with respect to launched pump power, although significantly improved efficiency is anticipated in an optimized system. Shorter cavities, in general, provide more robust single-frequency operation. Higher dopant concentration and higher reflectivity gratings would allow significantly shorter resonators, with a distributed feedback laser as a realistic ultimate prospect.

IX. CONCLUDING DISCUSSION

In this paper, we have presented modeling calculations which illustrate the wide range of performance that can be achieved using Ytterbium-doped silica fibers. The illustrative examples used in our discussion correspond mainly to experimental situations we have already investigated, and these examples confirm that the modeling provides a valuable guideline in designing Yb^{3+}-doped fiber lasers for specific uses. Neither the examples chosen nor the experimental investigations made to date can be said to represent an exhaustive coverage of the possibilities for Yb^{3+}-doped silica fiber lasers. Many aspects of lasing performance, such as

ultimate power-handling capability, need a great deal more investigation, and there is much more that can be done on optimization of performance. This includes optimization of various interdependent fiber parameters, such as maximizing dopant concentration and photosensitivity while minimizing background loss. Many future developments will capitalize on the continuing improvements being made in fiber grating performance, with exciting prospects for single-frequency lasers and high-power lasers over a significant spectral range over a significant spectral range, with 975 nm to 1180 nm demonstrated so far, and with prospects for further extension to longer wavelengths.

ACKNOWLEDGMENT

REFERENCES

[1] H. W. Etzel, H. W. Gandy, and R. J. Ginther, "Stimulated emission of infrared radiation from ytterbium-activated silicate glass," *Appl. Opt.*, vol. 1, pp. 534, 1962.

[2] M. E. Fermann, D. C. Hanna, D. P. Shepherd, P. J. Suni, and J. E. Townsend, "Efficient operation of an Yb-sensitised Er fiber laser at 1.56 μm," *Electron. Lett.*, vol. 24, pp. 1135–36, 1988.

[3] S. G. Grubb, W. F. Humer, R. S. Cannon, T. H. Windhorn, S. W. Vendetta, K. L. Sweeney, P. A. Leilabady, W. L. Barnes, K. P. Jedrzejewski, and J. E. Townsend, "+21 dBm erbium power amplifier pumped by a diode-pumped Nd:YAG laser," *IEEE Photon. Technol. Lett.*, vol. 4, no. 6, pp. 553–555, 1992.

[4] D. C. Hanna, R. M. Percival, I. R. Perry, R. G. Smart, P. J. Suni, and A. C. Tropper, "Yb-doped monomode fiber laser: broadly tunable operation from 1.010 μm to 1.162 μm and three level operation at 974 nm," *J. Modern. Optics*, vol. 37, pp. 329–331, 1987.

[5] J. R. Armitage, R. Wyatt, B. J. Ainslie, and S. P. Craig-Ryan, "An Yb^{3+}-doped silica fiber laser," *Electron. Lett.*, vol. 25, no. 5, pp. 298–299, 1989.

[6] J. Y. Allain, M. Monerie, and H. Poignant, "Ytterbium-doped fluoride fiber laser operating at 1.02 μm," *Electron. Lett.*, vol. 28, no. 11, pp. 988–989, 1992.

[7] C. J. Mackechnie, W. L. Barnes, D. C. Hanna, and J. E. Townsend, "High-power ytterbium (Yb^{3+})-doped fiber laser operating in the 1.12 μm region," *Electron. Lett.*, vol. 29, no. 1, pp. 52–53, 1993.

[8] J. Y. Allain, J. F. Bayon, M. Monerie, P. Bernage, and P. Niay, "Ytterbium-doped silica fiber laser with intracore Bragg gratings operating at 1.02 μm," *Electron. Lett.*, vol. 29, no. 3, pp. 309–310, 1993.

[9] P. Lacovara, H. K. Choi, C. A. Wang, R. L. Aggarwal, and T. Y. Fan, "Room-temperature diode-pumped Yb:YAG laser," *Opt. Lett.*, vol. 16, no. 14, pp. 1089–1091, 1991.

[10] T. Y. Fan, "Heat generation in Nd:YAG and Yb:YAG," *IEEE J. Quantum Electron.*, vol. 29, no. 6, pp. 1457–1459, 1993.

[11] P. St. J. Russell, J. L. Archambault, and L. Reekie, "Fiber gratings," *Phys. World*, pp. 41–46, Oct. 1993.

[12] Y. Ohishi, T. Kanamori, T. Kitagawa, S. Takahashi, E. Snitzer, and G. Sigel, "Pr^{3+}-doped fluoride fiber amplifier operating at 1.31 μm," *Opt. Lett.*, vol. 16, no. 22, pp. 1747–1749, 1991.

[13] R. G. Smart, D. C. Hanna, A. C. Tropper, S. T. Davey, S. F. Carter, and D. Szebesta, "CW room temperature upconversion lasing at blue, green, and red wavelengths in infrared-pumped Pr^{3+}-doped fluoride fiber," *Electron. Lett.*, vol. 27, no. 14, pp. 1307–1309, 1991.

[14] D. Piehler, D. Craven, N. Kwong, and H. Zarem, "Laser-diode-pumped upconversion fiber lasers," *Electron. Lett.*, vol. 29, no. 21, pp. 1857–1858, 1993.

[15] H. M. Pask, A. C. Tropper, D. C. Hanna, B. N. Samson, R. D. T. Lauder, P. R. Barber, L. Reekie, J. L. Archambault, S. T. Davey, and D. Szebesta, "Upconversion laser action in Pr^{3+}-doped ZBLAN fiber pumped by an Yb-doped silica fiber laser," *Adv. Solid-State Lasers*, Salt Lake City, UT, Tech. Dig., paper ATuD1-1, 1994, pp. 172–174.

[16] S. G. Grubb, K. W. Bennett, R. S. Cannon, and W. F. Humer, "CW room-temperature blue upconversion fiber laser," *Electron. Lett.*, vol. 28, pp. 1243–1244, 1992.

[17] P. R. Barber, C. J. Mackechnie, R. D. T. Lauder, H. M. Pask, A. C. Tropper, D. C. Hanna, S. D. Butterworth, M. J. McCarthy, J.-L. Archambault, and L. Reekie, "All solid-state blue room temperature Thulium-doped upconversion fiber laser," *Compact Blue-Green Lasers*, Salt Lake City, UT, Tech. Dig., paper CFA3-1, 1994, pp. 68–70.

[18] J. Hamel, A. Cassini, H. Abu-Safia, and M. Leduc, "Diode-pumping of LNA lasers for helium optical pumping," *Opt. Commun.*, vol. 63, pp. 114–117, 1987.

[19] T. Y. Fan and R. L. Byer, "Modeling and CW operation of a quasi-three level 946 nm Nd:YAG laser," *IEEE J. Quantum Electron.*, vol. QE-23, no. 5, pp. 605–612, 1987.

[20] G. Meltz, W. W. Morey, and W. H. Glenn, "Formation of Bragg gratings in optical fibers by a transverse holographic method," *Opt. Lett.*, vol. 14, no. 15, pp. 823–825, 1989.

[21] H. M. Pask, J.-L. Archambault, D. C. Hanna, L. Reekie, P. St. J. Russell, J. E. Townsend, and A. C. Tropper, "Operation of cladding-pumped Yb^{3+}-doped silica fiber lasers in the 1 μm region," *Electron. Lett.*, vol. 30, no. 11, pp. 863–864, 1994.

[22] V. P. Gapontsev, I. E. Smartsev, A. A. Zayat, and R. R. Loryan, "Laser diode pumped Yb-doped single-mode tunable fiber laser," *Adv. Solid-State Lasers*, Hilton Head, NC, Tech. Dig., paper WC1-1, March 1991, pp. 214–216.

[23] H. Po, E. Snitzer, R. Tumminelli, L. Zenteno, F. Hakimi, N. M. Cho, and T. Haw, "Doubly-clad high brightness Nd fiber laser pumped by GaAlAs phased array," in *Proc. OFC*, Houston, TX, paper PD7, 1989.

[24] J. D. Minelly, W. L. Barnes, R. I. Laming, P. R. Morkel, J. E. Townsend, S. G. Grubb, and D. N. Payne, "Diode-array pumping of Er^{3+}/Yb^{3+} co-doped fiber lasers and amplifiers," *IEEE Photon. Technol. Lett.*, vol. 5, no. 3, pp. 301–303, 1993.

[25] G. A. Ball, W. W. Morey, and W. H. Glenn, "Standing-wave monomode Erbium fiber laser," *IEEE Photon. Technol. Lett.*, vol. 3, no. 7, pp. 613–615, 1991.

[26] J. T. Kringlebotn, P. R. Morkel, L. Reekie, J.-L. Archambault, and D. N. Payne, "Efficient diode-pumped single-frequency erbium:ytterbium fiber laser," *IEEE Photonics Techn. Lett.*, vol. 5, no. 10, pp. 1162–1164, 1993.

[27] J. M. Dawes, H. M. Pask, J.-L. Archambault, J. E. Townsend, D. C. Hanna, L. Reekie, and A. C. Tropper, "Single frequency lasers and efficient cladding-pumped lasers using Yb^{3+}-doped silica fiber," *CLEO Europe*, paper CThJ1, 1994.

[28] S. V. Chernikov, J. R. Taylor, and R. Kashyap, "Coupled-cavity erbium fiber lasers incorporating fiber grating reflectors," *Opt. Lett.*, vol. 18, no. 23, pp. 2023–2025, 1993.

David C. Hanna was born in Nottingham, England in 1941. He received the B.A. degree from Cambridge University in 1962, and the Ph.D. degree from Southampton University in 1967.

He is currently a professor with the Department of Physics, and a Deputy Director of the Optoelectronics Research Centre, Southampton. He has spent periods of leave at the Politechnico di Milano Italy, and as an Alexander von Humboldt Fellow at the University of Munich, Munich, Germany. He is past chairman of the Quantum Electronics Group of the Institute of Physics, and was program chair for the CLEO-Europe Conference in 1994.

Dr. Hanna received the Max Born medal and prize from the German Physical Society. His present interests include optical fiber lasers, diode-pumped solid-state lasers, crystal waveguide lasers and optical parametric oscillators.

Anne C. Tropper was born in London in 1954. She studied at Somerville College, Oxford and the Clarendon Laboratory, receiving the D.Phil. degree in 1978.

She is currently a reader with the Department of Physics at the University of Southampton, partly seconded to the Optoelectronics Research Centre. Her interests include optical fiber lasers, upconversion fiber lasers, and crystal waveguide lasers.

Colin J. Mackechnie received the B.Sc. honors degree in physics from the University of Glasgow, Scotland in 1990, and the degree of Ph.D. from the University of Southampton, U.K. in 1994.

In 1992 he became a director of Quinag Ltd. Currently, he is an A.S.I. Visiting Fellow at the University of Victoria, B.C., Canada, and at Seastar Optics, Inc., Sidney, B.C., Canada.

H. M. Pask, photograph and biography not available at the time of publication.

Robert J. Carman was born in Kingston-upon-Thames, England in 1959. He received the B.Sc. honors degree in physics from Manchester University, England in 1981, and the Ph.D. degree from the University of St. Andrews, Scotland in 1986. His dissertation was on electron beam generation in low pressure glow discharges for the excitation of continuous wave gas lasers.

After receiving the Ph.D. degree, he held a postdoctoral research position at the University of Southampton, England on ejected-electron spectroscopy of metal atoms. He was a visiting scientist at Massey Universtiy, New Zealand in 1986, before joining the Centre for Lasers and Applications at Macquarie University, Sydney, Australia, as a Postdoctoral Research Fellow in 1987. He was also a British Council visiting Research Fellow in the Optoelectronics Research Centre at Southampton University in 1992. In 1994 he became an Australian Research Fellow, and is currently working on the development of computer models for high-power gas laser systems in the visible and IR regions. His research interests include gaseous electronics, lasers, atomic collisions, plasma diagnostics and spectroscopy, low pressure discharges, non-equilibrium electron transport, optical fiber lasers, and numerical modeling relating to lasers, discharges, and plasmas.

Dr. Carman is a member of the Institute of Physics, U.K.

Paul R. Barber was born in Ipswich, England in 1970. He received the B.Sc. honors degree in physics with optoelectronics from the Universtiy of Southampton, England in 1992.

He is currently a research student working within the Optoelectronics Research Centre at the same location. His research interests include the use of doped optical fibers as laser sources and amplifiers.

Judith M. Dawes received the B.Sc. honors degree in physical chemistry in 1983, and the Ph.D. degree in 1989 from the University of Sydney, Sydney, Australia.

After postdoctoral research at the Ontario Laser and Lightwave Research Centre, University of Toronto, Canada, she joined the Centre for Lasers and Applications, Macquarie University, Sydney, as a Research Fellow, working on diode pumped solid-state lasers. She is currently a senior lecturer in the School of Mathematics, Physics, Computing, and Electronics at Macquarie University, with research interests in developing solid-state lasers for remote sensing and microsurgery.

Dr. Dawes is a member of the Optical Society of America, the Australian Optical Society, and the American Physical Society.